A&A 410, 155–164 (2003)
DOI: 10.1051/0004-6361:20031131

Astronomy & Astrophysics

Near-IR [Fe II] emission diagnostics applied to cold disk winds in young stars

N. Pesenti[1], C. Dougados[1], S. Cabrit[2], D. O'Brien[3], P. Garcia[3], and J. Ferreira[1]

[1] Laboratoire d'Astrophysique UMR 5571, Observatoire de Grenoble, BP 53, 38041 Grenoble Cedex 9, France
[2] LERMA, Observatoire de Paris, UMR 8112 du CNRS, 61 avenue de l'Observatoire, 75014 Paris
[3] Centro de Astrofísica da Universidade do Porto, Rua das Estrelas, 4150-762 Porto, Portugal

Received 9 April 2003 / Accepted 12 June 2003

Abstract. We investigate the emissivity properties of the main near-IR transitions of the Fe^+ ion in the conditions prevailing in the inner regions of jets from young stars, based on a simplified 16-level atom model. We present new diagnostic diagrams involving prominent near-IR line ratios that allow us to constrain the electronic density, temperature, and Fe gas phase abundance ratio, independently of the heating process. Comparison with recent near-IR observations of a sample of HH objects indicates gas phase Fe abundances ranging from 15–50% up to 100% of the solar value (depending on the assumed temperature and on the HH object), in agreement with the moderate depletions previously derived from optical line ratios or shock models. Hence, it appears that Fe-bearing dust is efficiently destroyed in stellar jets. We then use our Fe^+ emissivity model to predict near-IR [Fe II] emission maps for self-similar, cold MHD disk wind models. We show that near-IR [Fe II] lines are stronger than [S II] λ6731 and [O I] λ6300 in the cool regions ($T \leq 7000$ K) near the wind base, and that observations in [Fe II] with AMBER on the VLTI could severely constrain the MHD solution and the inner launch radius of the jet. We also compare theoretical predictions with recent observations in the near-IR [Fe II] lines of the L1551-IRS5 and DG Tau jets. The cold disk wind model reproduces quite well the two velocity components observed at −100 and −300 km s^{-1}, although the high velocity component appears overestimated by a factor of 1.5 in the DG Tau jet. However, the model predicts too little emission at intermediate velocities and insufficient densities. Similar problems were encountered in previous model comparisons in the optical range with jets from T Tauri stars. Denser disk winds with stronger heating at the jet base, which have been invoked for optical jets, also appear needed in younger, embedded Class I jet sources.

Key words. ISM: jets and outflows – stars: formation – ISM: Herbig-Haro objects – infrared: ISM

1. Introduction

Constraining the physical mechanism by which mass is ejected from young accreting stars and collimated into jets remains a fundamental open problem in star formation theory. The fact that a correlation between accretion and ejection signatures is seen from the embedded Class 0 and Class I phases (ages a few 10^4–10^5 yr) down to the optically revealed T Tauri phase (at ages a few 10^6 yr), with a similar ejection to accretion ratio, suggests that the same mass-loss mechanism may be at play throughout the different stages of star formation (see e.g. Cabrit 2002). Studies of the inner jet structure at each phase of evolution are required to confirm the validity of this scenario. Attempts to compare observations and MHD wind predictions have first concentrated on the small scale jets associated with optically revealed T Tauri stars (Cabrit et al. 1999; Garcia et al. 2001a,b; Lavalley-Fouquet et al. 2000; Bacciotti et al. 2000; Shang et al. 1998, 2002). These studies are conducted in the strong optical forbidden lines of [O I] λ6300, [S II] λ6731 and [N II] λ6584. Thanks to recent advances in near-IR instrumentation, similar work can now be extended to the inner regions of jets associated with the younger more extincted Class I sources.

The imaging study of embedded jet sources with NICMOS/HST made by Reipurth et al. (2000) clearly demonstrated the importance of [Fe II] near-IR lines as a tracer of the innermost jet regions, less affected by extinction than their optical counterparts. Furthermore, Nisini et al. (2002) recently performed a near-IR spectroscopic survey (from 0.95 to 2.5 μm) of a sample of HH jets, providing a first database to investigate the excitation conditions of the Fe^+ ion in young stellar jets. Detailed modeling is now needed to see how such observations can be used to constrain the jet driving mechanism in embedded sources.

We investigate in this article the emissivity properties of the main near-IR lines of the Fe^+ ion, based on a simplified 16-level model, in the conditions prevailing in the inner regions of jets from young stars. Extending the work of Nisini et al. (2002) and Beck-Winchatz et al. (1994), we first derive in Sect. 2 diagnostic diagrams that allow to constrain,

---

Send offprint requests to: N. Pesenti,
e-mail: `Nicolas.Pesenti@obs.ujf-grenoble.fr`

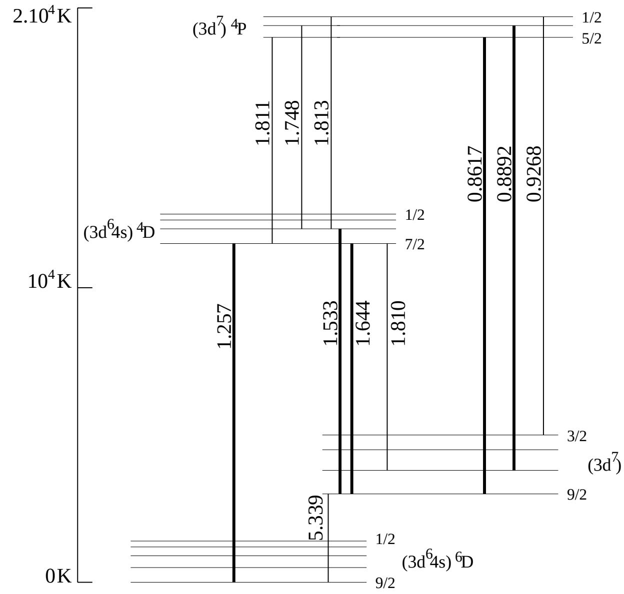

Fig. 1. Energy level diagram with the prominent optical and near-infrared [Fe II] emission lines (wavelengths in μm) originating from the 16 first low-lying levels. We also indicate on the left the range of corresponding upper level energies (E/k expressed in K).

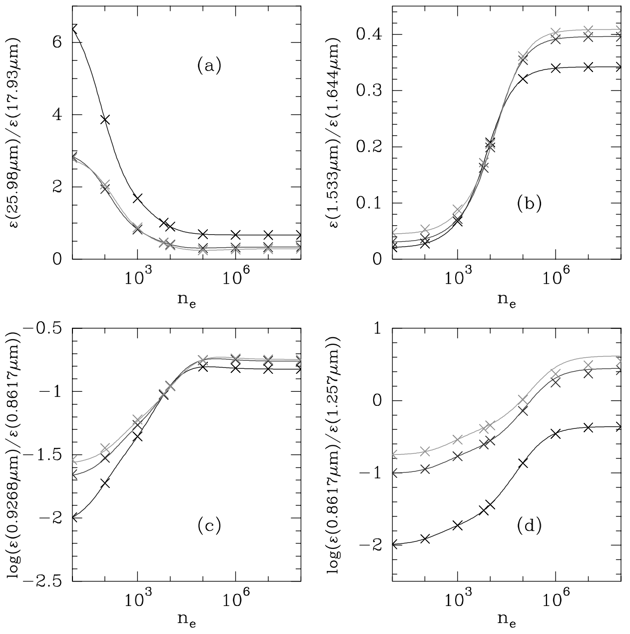

Fig. 2. Theoretical line ratios as a function of n_e for different temperature values T_e (3000, 10 000, 20 000 K). The curves are deduced from our 16-level model and symbols from a 142-level computation (Pradhan, private communication). T_e increases from bottom to top in panels **b)**, **c)** and **d)**, from top to bottom in panel **a)**.

independently of the heating process and ejection model, the electronic temperature and density as well as the Fe^+/S^+ gas phase abundance ratio – a critical parameter to derive mass loss rates from [Fe II] line fluxes and to estimate the amount of depletion onto dust grains. We then turn in Sect. 3 to detailed predictions for a specific class of ejection model, the self-similar cold disk wind solutions developed by Ferreira (1997), for which consistent thermal solutions have been recently computed by Garcia et al. (2001a). Our study extends the work of Garcia et al. (2001b), which was restricted to the optical domain. We compare these predictions with recent observations in near-IR [Fe II] lines of young stellar jets from embedded sources, in particular the velocity resolved spectroscopy of the inner regions of the L1551-IRS5 (Pyo et al. 2002) and the DG Tau jets (Pyo et al. 2003). We summarize our findings in Sect. 4.

2. Near-IR [Fe II] diagnostic diagrams

2.1. The 16-level Fe^+ model

To predict near-IR [Fe II] line emissivities, we build a NLTE model including the 16 first fine structure levels, which comprise the 4 terms $(3d^64s)^6D$, $(3d^7)^4F$, $(3d^64s)^4D$, $(3d^7)^4P$ (Fig. 1). Levels in the ^4P multiplet lie ~1.7 eV above the ground state so that our simplified model will be valid for excitation temperatures below 2×10^4 K, a condition typically achieved in stellar jets (see below). All radiative transitions among these four terms are of quadrupole or magnetic dipole type. We therefore assume optically thin conditions and compute level populations under statistical equilibrium including electron collisional excitation and spontaneous radiative emission processes. We take transition probabilities from Nussbaumer & Storey (1988), level energies and electron-ion collision strengths from Zhang & Pradhan (1995). We neglect fluorescent excitation by the UV continuum of the star. Indeed, as pointed out by Verner et al. (2000) in the case of the Orion Nebula, the 16 lowest levels of the Fe^+ ion remain collisionally dominated in the conditions under study (optically thin emission, $n_e = 1$–10^8 cm^{-3}, $T_e \sim 10^4$ K). Thus, the line emissivity per Fe^+ ion only depends on electron density (n_e) and temperature (T_e).

We have tested our simplified model by comparing our results with a more accurate 142-level computation, taking into account the same physical processes (Pradhan, private communication). The comparison is shown in Fig. 2 for the same four line ratios as in Pradhan & Zhang (1993), which probe all four lowest terms of Fe^+. Our predicted line ratios are in very good agreement with those obtained from the 142-level model, for n_e ranging from 10 to 10^8 cm^{-3} and T_e ranging from 3000 to 2×10^4 K. Differences do not exceed 1% except for transitions originating from the upper ^4P level (e.g. 0.8617 μm, 0.9268 μm) and $T_e > 10\,000$ K, where our model underestimates the 0.8617 μm/1.257 μm ratio by up to 5% for $n_e \leq 10^5$ cm^{-3}, and by ~20% for $n_e > 10^5$ cm^{-3}. These differences still remain below current observational uncertainties in line ratios. Our simplified 16-level model is thus sufficiently accurate for diagnostic purposes.

In the following, we concentrate on the prominent optical and near-infrared lines. Most of the brightest transitions arise from the ^4D term, namely 1.257 μm, 1.644 μm and 1.533 μm (Fig. 1). The decay $^4F_{9/2}$–$^4P_{5/2}$ (0.8617 μm) or $^6D_{9/2}$–$^4F_{9/2}$ (5.339 μm) lines also have significant emissivities (≥one tenth of the 1.257 μm line). The latter is inaccessible from ground-based telescopes but may be observable from space, with JWST for example.

Table 1. Critical densities ($n_{\rm cr}$) of upper levels for the prominent atomic transitions, calculated using Eq. (1) for $T_{\rm e}$ = 5000 K and 10 000 K.

Level	Transition	$n_{\rm cr}$ (cm^{-3}) 5000 K	$n_{\rm cr}$ (cm^{-3}) 10 000 K
[Fe II] $^4D_{9/2}$	1.644, 1.257 μm	3.5×10^4	5.6×10^4
[Fe II] $^4D_{7/2}$	1.533 μm	2.9×10^4	4.6×10^4
[Fe II] $^4P_{5/2}$	0.8617 μm	2.6×10^5	3.5×10^4
[O I] $^1D_2$	0.6300 μm	4.6×10^6	1.8×10^6
[S II] $^2D_{3/2}$	0.6731 μm	2.7×10^3	3.5×10^3

2.2. Derivation of ($n_{\rm e}$, $T_{\rm e}$)

Critical densities for the most intense [Fe II] lines, and for the main forbidden lines of [S II] and [O I] observed in jets, can be calculated with the generalized formula of Osterbrock (1989):

$$n_{\rm cr}(i) = \Sigma_{j<i} A_{ij} / \Sigma_{j \neq i} q_{ij}, \qquad (1)$$

where A_{ij} denotes Einstein spontaneous emission coefficients and q_{ij} denotes collisional rate coefficients. The results are given in Table 1, and show that the [Fe II] lines investigated here have critical densities of a few 10^4 cm^{-3} (slightly higher than the red [S II] $\lambda\lambda$6716, 6731 lines[1]). They will therefore probe emitting regions with electronic densities of the same order. Line ratios involving transitions with similar excitation energies and similar ground states can be used to derive $n_{\rm e}$. For $n_{\rm e}$ in the range 10^2 to 10^5 cm^{-3}, the best diagnostic is the [Fe II] 1.644 μm/1.533 μm ratio. Indeed, this ratio involves two of the brightest near-IR [Fe II] lines and is little dependent on temperature and reddening (Fig. 2b). Note that the brightest two transitions at 1.644 and 1.257 μm originate from the same upper level. Their ratio (ϵ(1.257 μm)/ϵ(1.644 μm) = 1.36) is therefore insensitive to the excitation conditions and can be used to derive the extinction $A_{\rm V}$ along the line of sight.

Since most of the prominent near-infrared transitions have similar excitation energies, their ratio is not very sensitive to the gas temperature. Combining them with transitions from the ^{4}P term, with higher excitation energy, could in principle lead to gas temperature determinations. In the near-infrared domain, the transitions at 1.811 μm and 1.813 μm would be very good candidates. However, these lines lie in a region of poor atmospheric transmission and in addition are blended with the stronger ^{4}F–^{4}D 1.810 μm line. The line at 1.748 μm is weaker and may be, at the present available spectral resolutions, strongly contaminated by the H_2 1–0 S(7) transition (cf. Nisini et al. 2002). A few lines lying in the red part of the optical spectrum can be used, the most prominent being at 0.8617 μm and 0.8892 μm. In Fig. 3, we propose a diagnostic diagram, combining the density sensitive [Fe II] 1.644 μm/1.533 μm ratio with the temperature sensitive [Fe II] 0.8617 μm/1.257 μm ratio, which provides a direct measure of ($n_{\rm e}$,$T_{\rm e}$). A similar diagram, including the red transition at $^4F_{3/2}$–$^4P_{3/2}$ 0.9471 μm, is proposed in Nisini et al. (2002). With a flux ratio uncertainty of ±10% for the [Fe II] 1.644 μm/1.533 μm ratio, the diagnostic diagram presented in Fig. 3 would allow determination of $n_{\rm e}$ ranging from 10^2 to 10^5 cm^{-3} with less than a factor 4 uncertainty (total error). To achieve an uncertainty of ±15% on $T_{\rm e}$ at $T_{\rm e} \lesssim$ 10 000 K, an estimated error of ±15% in the [Fe II] 0.8617 μm/1.257 μm ratio is required.

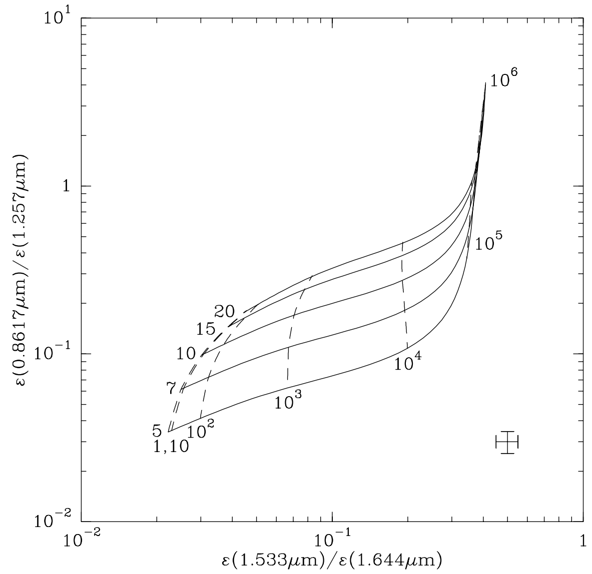

Fig. 3. Diagnostic diagram of ($n_{\rm e}$,$T_{\rm e}$): temperature sensitive ratio 0.8617 μm/1.257 μm versus electronic density sensitive ratio 1.533 μm/1.644 μm. **Dashed lines**: $n_{\rm e}$ varying from 1 to 10^6 cm^{-3} in factors of 10. **Solid lines**: $T_{\rm e}$ varying from 5000 to 20 000 K ($T_{\rm e}$ expressed in factors of 10^3 K). Error bars correspond to typical uncertainties of ±10% and ±15% in 1.533 μm/1.644 μm and 0.8617 μm/1.257 μm respectively.

2.3. Diagnostic of gas phase Fe abundance

In the interstellar medium, condensation processes onto dust grains deplete the gas phase abundance of heavy elements such as Fe by a factor >10 (Savage & Sembach 1996). In jets from young stellar objects, sputtering processes in sufficiently fast shocks (see e.g. Jones et al. 1994) could destroy a significant fraction of the dust grains, replenishing the gas phase with heavy elements. Strong heating at the jet base could also evaporate dust grains in the ejected gas. The gas phase abundance of Fe in HH flows is therefore an important parameter giving interesting indications on the shock and thermal history of ejected matter. In addition, estimates of the Fe^+ gas phase abundance in HH flows are critically required to derive mass-loss rates from [Fe II] line fluxes.

A first method to assess the iron gas phase depletion consists in comparing the Fe abundance to that of sulfur, an element not significantly depleted onto dust grains, with a known gas-phase abundance of 1.86×10^{-5} (Savage & Sembach 1996). In young stellar jets, emission of these elements is dominated by [Fe II] and [S II] lines. However, the Fe^+/S^+ ratio derived

---

[1] The critical density for the [S II] λ6731 line in Table 1 is markedly lower than the value $\simeq 10^4$ cm^{-3} often quoted in the literature, derived from a two-level atom approximation.

from these lines is probably very similar to the total Fe/S ratio. If the lines are formed in cooling flows behind shock waves, one expects $Fe^+/Fe \leq S^+/S \leq 2Fe^+/Fe$ (Beck-Winchatz et al. 1996), so that $Fe^+/S^+ \leq Fe/S \leq 2Fe^+/S^+$. If jet heating is instead dominated by ambipolar diffusion and UV radiation from the accretion shock, S and Fe should be both predominantly in their singly ionized form (see Garcia et al. 2001a), so that $Fe/S = Fe^+/S^+$. In either case, the Fe^+/S^+ ratio provides a valuable lower limit to the actual Fe/S ratio, within a factor of 2 of the true value.

This method was first applied to HH objects by Beck-Winchatz et al. (1994,1996), using a large sample of optical [Fe II] lines. The Fe^+/S^+ ratio is derived from the relative intensities of [Fe II] and [S II] optical lines by means of a statistical equilibrium model, similar to that outlined in Sect. 2.1, given appropriate values of (n_e,T_e). The assumption of a uniform emission region is partly justified by the fact that the lines are excited under rather similar conditions (see Sect. 2.2). Inferred gas phase Fe^+/S^+ ratios range from 1 to 4 when the [S II] $\lambda\lambda 6716, 6731$ lines are used for reference. When compared with the most recent estimate of the solar Fe/S ratio ≃1.7, consistent with the local ISM (Savage & Sembach 1996; Sofia & Meyer 2001), these values indicate no Fe gas phase depletion in most HH flows. Surprisingly, no correlation with the degree of excitation of the flow is observed. This analysis was however limited to the case of optically revealed parts of the jets, i.e. usually far from the driving source.

Recently, Nisini et al. (2002) proposed two other methods to measure the Fe gas phase abundance in young stellar jets, relying only on near-infrared lines. The first one involves the [Fe II] 1.257 μm/Paβ ratio, assuming that Paβ is emitted under case B recombination. A drawback of this method is that, in addition to n_e and T_e, it requires knowledge of the hydrogen ionization fraction, x_e, which is not available for all sources. Furthermore, the assumption that Paβ is formed in the same region as [Fe II], and that it is dominated by recombination, is generally not valid in shocks (cf. Bacciotti & Eislöffel 1999). A second method proposed by these authors is to compare the observed near-IR line ratios [Fe II] 1.257 μm/[C I] 0.98 μm and [Fe II] 1.257 μm/Paβ with predictions from models of fast dissociative shocks. In the sample of objects studied by Nisini et al. (2002), the inferred gas phase Fe/H ranges from 30% to 70% of the solar photospheric value ($(Fe/H)_\odot = 3.2 \times 10^{-5}$, Savage & Sembach 1996). These results depend on the assumption that the carbon abundance in the shock remains constant at 2.3×10^{-4}, i.e. 64% of the solar value (Hollenbach & McKee 1989; Savage & Sembach 1996), while Fe is returned to the gas phase. A solar gas-phase carbon abundance would increase their estimated Fe/H by typically a factor 1.5.

We propose here a third approach to estimate the gas phase Fe abundance of HH flows from near-IR observations, independent of both x_e and shock models. The method is simply an extension to the near-IR domain of that introduced by Beck-Winchatz et al. (1994) in the optical range. As described above, it will yield a lower limit to the Fe/S ratio. We propose to use the ratio of the [Fe II] 1.257 μm line to the [S II] 1.029 + 1.032 + 1.034 + 1.037 μm lines (hereafter referred to as [S II] 1.03 μm). We predict comparable integrated flux in these lines in the conditions under study and, indeed, these near-IR [S II] lines have been detected by Nisini et al. (2002) in their sample of HH objects. We have chosen the [Fe II] 1.257 μm line because it is one of the brightest transitions and it minimizes reddening uncertainties relative to [S II] 1.03 μm. To compute the emissivity per ion for S^+, we construct a model including the 5 low-lying metastable levels. Transition probabilities are taken from Fritzsche et al. (1999), collision strengths from Cai & Pradhan (1993). We also use the [Fe II] 1.533 μm/1.644 μm ratio, as an indicator of n_e. Figure 4 presents the resulting diagnostic diagram, which plots [S II] 1.03 μm/[Fe II] 1.257 μm versus [Fe II] 1.533 μm/1.644 μm, and yields the gas phase Fe^+/S^+ ratio provided T_e is known. It can be seen that near-IR [Fe II]/[S II] line ratios are more sensitive to temperature than the optical ratios (see Table 2 of Beck-Winchatz et al. 1994), though they are less sensitive to reddening.

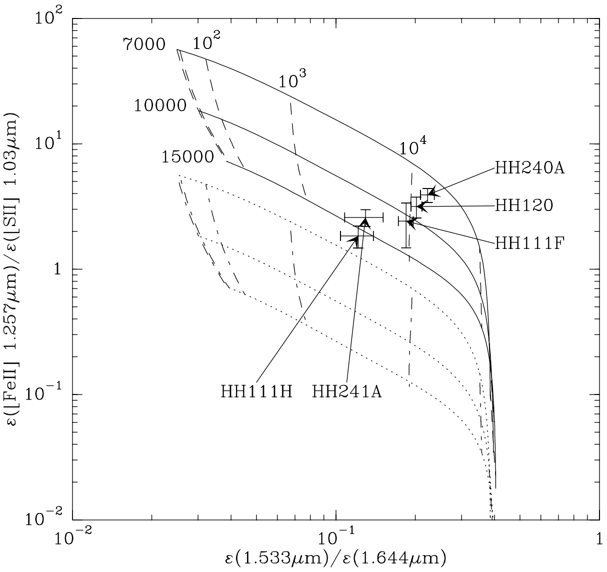

Fig. 4. Diagnostic diagram of the Fe^+/S^+ gas phase abundance. We plot the density sensitive ([Fe II] 1.533 μm/1.664 μm) ratio versus the depletion sensitive [Fe II] 1.257 μm/([S II] (1.029 + 1.032 + 1.034 + 1.037) μm ratio. Predicted line ratios are plotted as function of T_e (solid lines) and n_e (dashed lines) for $Fe^+/S^+ = 1.7$ (corresponding to solar abundances, Savage & Sembach 1996). Dotted and dash-dotted lines correspond to $Fe^+/S^+ = 0.17$ (1/10 of solar value). Observed line ratios for the sample of HH objects studied by Nisini et al. (2002), corrected for individual reddenings, are represented with their error bars (including A_V uncertainties).

We plot in Fig. 4 the observational data from Nisini et al. (2002). Temperatures are not available for these sources, but a range of 7000 to 15 000 K can be safely assumed, based on the predicted temperature of the low excitation forbidden line emitting region in planar shock models on the one hand (Hartigan et al. 1994), and maximum derived temperatures in optically visible HH flows, on the other hand (Böhm & Solf 1990). We can derive an absolute *lower limit* to the Fe^+/S^+ gas phase ratio, and hence to the Fe/S ratio, by assuming T_e = 7000 K. These limits are: 0.25 ± 0.1 for HH 111H, 0.39 ± 0.1 for HH 241A, 0.55±0.2 for HH 111F, 0.83±0.15 for HH 120H, and 1.2 ± 0.25 for HH 240A, and range from ≃15% to 70%

of the solar value (Fe/S = 1.7). These values are remarkably similar to the results found by Nisini et al. (2002) from shock models, with the same ordering for the 5 individual sources. However, we stress that the above estimates are lower limits. With $T_e \simeq 10^4$ K, the data are compatible with no depletion in most sources, except HH 241A and HH 111H (50% depletion). In the following, we will thus make the assumption that all iron is in the gas phase. However, we point out that to derive iron depletion and jet mass-loss rates to better than a factor ≃5 from [Fe II] line fluxes, T_e estimates will be critically required.

3. Predictions for cold MHD disk winds

In this section, we use our simplified Fe$^+$ model to predict near-IR [Fe II] emissivities for the class of self-similar MHD cold disk wind models developed by Ferreira (1997), for which fully consistent thermal solutions have been recently computed (Garcia et al. 2001a). We extend here the work presented in Garcia et al. (2001b), which was restricted to predictions in the optical domain. We first briefly describe the model and compare predicted emissivities in the near-IR [Fe II] lines with those of the prominent optical [O I] λ6300 and [S II] λ6731 emission lines. We then compare these predictions with recent observations in the near-IR domain of the stellar jets from L1551-IRS5 and DG Tau.

3.1. Wind model

The MHD accretion-ejection structures of Ferreira (1997) represent an improvement on the centrifugal MHD disk winds first calculated by Blandford & Payne (1982). Both assume that (1) matter is ejected along a large scale bipolar magnetic field threading through the accretion disk, (2) jet enthalpy is negligible for accelerating the flow (the wind is "cold"), and (3) the structure is steady-state, axisymmetric, and self-similar with the disk radius. However, the solutions of Ferreira (1997) also describe self-consistently the accretion flow in the underlying resistive Keplerian disk, including all relevant dynamical terms that govern the wind mass-loading at the slow-point (see Ferreira & Pelletier 1995). This global description imposes additional constraints on the self-similar structure, which is then specified by only three dimensionless parameters: (1) $\xi \equiv \mathrm{d}\log\dot{M}_{\rm acc}/\mathrm{d}\log r$, the ejection efficiency parameter, which is related to the total ejection/accretion ratio by $\dot{M}_{\rm ejec}/\dot{M}_{\rm acc} = \xi \times \ln(r_{\rm e}/r_{\rm i})$, where $r_{\rm e}$ and $r_{\rm i}$ are the outer and inner radii of the MHD disk-wind structure, (2) $\epsilon = h/r_0$, where h is the disk scale height at the cylindrical radius r_0, and (3) $\alpha_{\rm m} = \nu_{\rm m}/V_{\rm A}h$, where $\nu_{\rm m}$ is the required turbulent magnetic diffusivity and $V_{\rm A}$ is the Alfvén velocity on the disk midplane.

Following Cabrit et al. (1999), we will adopt $\epsilon = 0.1$ (as estimated in HH 30 by Burrows et al. 1996) and $\alpha_{\rm m} = 1$. Solutions that extend far from the Alfvén surface are then found for ξ between 0.005 and 0.012 (Ferreira 1997). We concentrate here on the solution with $\xi = 0.01$ (Model A in Cabrit et al. 1999), which is found to best reproduce the collimation properties of T Tauri microjets (Cabrit et al. 1999; Dougados et al. 2000). As a result of toroidal magnetic fields, the streamlines slowly recollimate beyond $z/r_0 \simeq 1500$ (where r_0 is the initial radius of the streamline in the disk), and terminate at $z/r_0 \simeq 8000$, due to strong refocusing towards the axis. One expects that a more gradual recollimation would occur in reality, due to additional pressure on the flow axis from open stellar magnetic field lines.

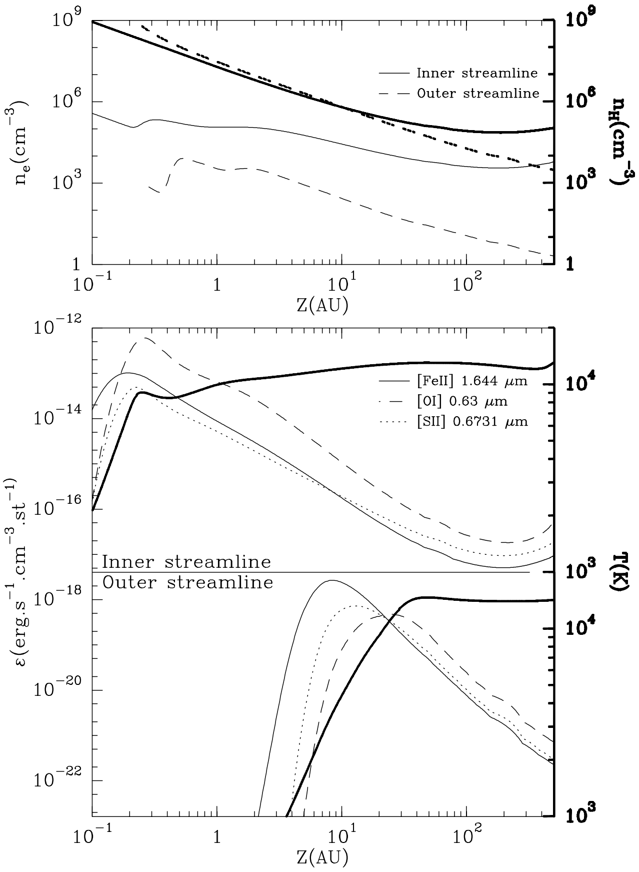

Fig. 5. Top: Variation of n_e and n_H (bold curve) along the inner (r_0 = 0.07 AU, full lines) and outer (r_0 = 1 AU, dashed lines) streamlines of the fiducial cold disk wind solution (ξ = 0.01, $\dot{M}_{\rm acc} = 10^{-6}\ M_\odot\,{\rm yr}^{-1}$, $M_* = 0.5\ M_\odot$) as a function of the altitude Z above the disk. **Middle and bottom**: Variation of line emissivities along the inner and outer streamlines for the 3 emission lines: [Fe II] 1.644 μm, [S II] λ6731 and [O I] λ6300. The variation of T_e is also shown in bold curve.

3.2. Predicted [Fe II] emissivities

The thermal and ionization structure of the MHD disk wind solutions of Ferreira (1997) was computed a posteriori by Garcia et al. (2001a) for an atomic gas of solar composition, along 11 streamlines anchored in the disk at radii ranging from r_0 = 0.07 AU, the typical disk corotation radius for a T Tauri star, to 1 AU, where molecules should start to form. The dominant heating mechanism is ambipolar diffusion, while adiabatic expansion dominates the cooling. We will use their results for a central stellar mass $M_* = 0.5\ M_\odot$ and accretion rates $\dot{M}_{\rm acc} = 10^{-5}$–$10^{-6}\ M_\odot\,{\rm yr}^{-1}$. We compute the emissivities in the [Fe II] near-IR lines along each streamline with the 16-level atom model described in Sect. 2.1, using the n_e, T_e and Fe$^+$/Fe ratios provided by the thermal solution.

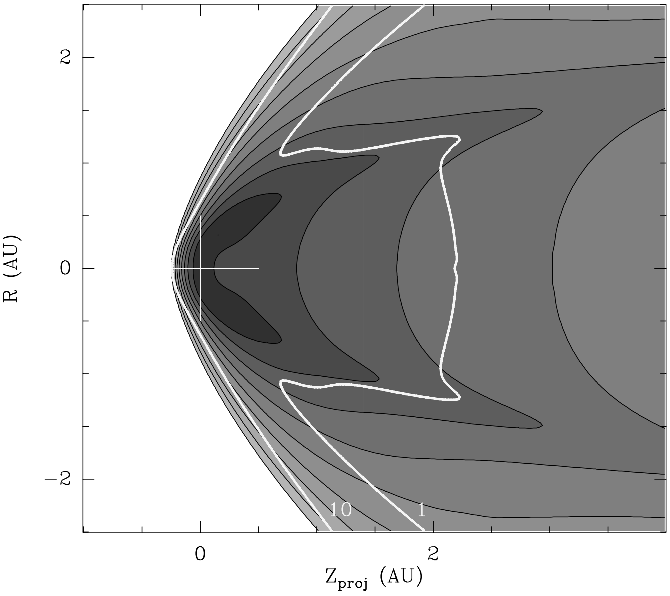

Fig. 6. Predicted [Fe II] 1.644 μm emission map of the fiducial cold disk wind solution with $\xi = 0.01$, $\dot{M}_{\rm acc} = 10^{-6}$ $M_\odot$ yr^{-1} and inclination to the line of sight i of 45°. The field of view (0.04″) and the Gaussian beam (1 mas, i.e. 0.14 AU) correspond to the AMBER/VLTI instrument characteristics. Filled contours start at the maximum surface brightness (2.3×10^{-4} W m^{-2} st^{-1}) and decrease by factors of 2. White contours correspond to [Fe II] 1.644 μm/[S II] λ6731 ratios of 10 and 1 (from left to right). The shape of the innermost streamline, assumed here anchored at 0.07 AU, is fully resolved and would set strong constraints on proposed MHD models.

The emissivity grid is projected onto the plane of the sky to construct emission maps and long slit spectra. Maps are then convolved by a two-dimensional Gaussian beam, representative of the instrumental spatial and spectral resolutions.

We first compare predicted near-IR [Fe II] emissivities along the flow with those predicted for the main optical emission lines of [S II] and [O I]. We plot in Fig. 5 the variation of emissivity with altitude along the innermost and outermost streamlines for the [Fe II] 1.644 μm, [S II] λ6731 and [O I] λ6300 lines. Both streamlines follow the same behavior in all 3 lines: emissivity first increases due to the central rise in temperature, the plasma then reaches a temperature plateau ($\sim 10^4$ K) and the drop in $n_{\rm e}$, due to the widening of the jet, produces the subsequent emissivity decrease. The final increase in the inner streamline at $Z > 200$ AU is due to compression in the recollimation zone. Since solutions have a self-similar geometry, maximum emissivity is reached at a lower altitude ($Z < 1$ AU) in the inner streamline as compared to the outer one ($Z \sim 10$ AU).

There are however important differences in emissivity profile between the 3 lines close to the central source. The upper level energies of near-IR [Fe II] lines ($E/k \sim 10\,000$ K) are lower than for [S II] λ6731 and [O I] λ6300 lines ($E/k \sim 20\,000$ K), so that the [Fe II]/[S II] and [Fe II]/[O I] ratios increase dramatically at the moderate electron temperatures $\leq$7000 K prevailing at the wind base. [Fe II] lines therefore appear to be a choice tracer for the cooler, dense regions at the wind base, typically below a few AUs. In addition, these near-IR lines would allow to better trace extincted regions at the base of embedded young stellar jets.

The AMBER/VLTI instrument, with a spatial resolution of $\simeq$1 mas (0.14 AU in Taurus) in the near-IR, will be ideally suited for such studies of innermost jet regions. We plot in Fig. 6 the predicted AMBER/VLTI map in [Fe II] 1.644 μm for our fiducial cold disk wind model, with $\dot{M}_{\rm acc} = 10^{-6}$ $M_\odot$ yr^{-1} and inclination angle to the line of sight of 45°. We also show as white contours the ratio of the [Fe II] 1.644 μm to the [S II] λ6731 surface brightnesses. As expected, the [Fe II] line is several times stronger than the [S II] one on scales $\leq$2 AU above the disk, due to the drop in $T_{\rm e}$. At this spatial resolution, the [Fe II] map is dominated by the innermost streamline, which is fully resolved, and shows a clear central hole. Hence, such observations could provide direct constraints on the shape (Z(r)) of the streamlines in the MHD jet solution and on the innermost radius at which ejection occurs.

3.3. Comparison with L1551-IRS5 and DG Tau

In this section, we discuss constraints on the ejection mechanism brought by recent observations in near-IR [Fe II] lines of the L1551-IRS5 and DG Tau jets. We compare these observations with predictions from our fiducial cold disk wind model and with constraints derived from previous studies of T Tauri jets in the optical domain.

3.3.1. Morphology and kinematics

One of the best-known young stellar jets is associated with the embedded binary source L1551-IRS5. It was first detected in the optical by Cohen et al. (1982). High resolution images show two extended ridges, identified as two separate jets with differing line of sight velocities (Fridlund & Liseau 1998; Itoh et al. 2000). Pyo et al. (2002) present velocity-resolved [Fe II] 1.644 μm spectra towards the base of the northern jet. These observations provide detailed morphological and kinematical information on the inner 500 AU of the jet, which can be directly compared to predictions from the cold disk wind model investigated here.

We adopt for the model an accretion rate of $\dot{M}_{\rm acc} = 10^{-5}$ $M_\odot$ yr^{-1} close to the estimated value for the L1551-IRS5 source of 6×10^{-6} $M_\odot$ yr^{-1} (Momose et al. 1998), an inclination angle to the line of sight of 45° (Pyo et al. 2002), and a central stellar mass of 0.5 $M_\odot$, i.e. roughly half the total mass of the binary system $\simeq$1.2 $M_\odot$ estimated from orbital motions (Rodriguez et al. 2003). Predicted emission maps and position-velocity (PV) diagrams are convolved with Gaussian beams of widths 0.3″ and 60 km s^{-1}, corresponding to the instrumental spatial and spectral resolutions of the L1551 observations.

Figures 7a,b,c present a comparison of observed and predicted maps in the [Fe II] 1.644 μm line. We also show in Fig. 7d synthetic maps taking into account the strong extinction observed towards L1551-IRS5. We artificially dimmed the predicted maps, before convolution with the instrumental beam, by a uniform screen of $A_{\rm V} = 20$ mag extending out to 1″, following the extinction measurements of Itoh et al. (2000).

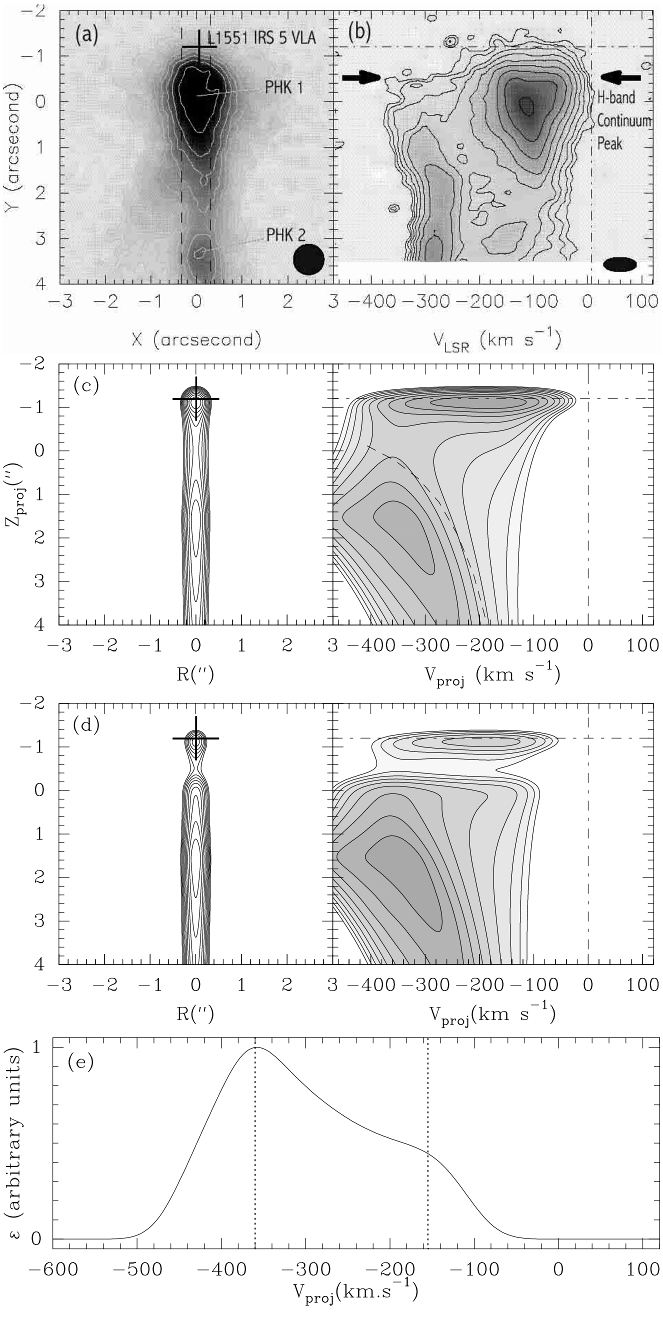

Fig. 7. [Fe II] 1.644 μm emission maps (*Left*) and position-velocity diagrams along the jet (*Right*). **a), b)** Observations of the L1551 jet from (Pyo et al. 2002) with a seeing size of 0.3″ and a velocity resolution of 59 km s^{-1}. **c)** synthetic maps predicted for a cold disk wind model with $\xi = 0.01$, $\dot{M}_{\rm acc} = 10^{-5}\ M_\odot\,{\rm yr}^{-1}$, $i = 45°$, convolved with the beam sizes of the L1551 observations. The cross and dot-dashed lines locate the position of IRS5 VLA as in the top panel. The dashed line traces the locus where streamlines start to recollimate (beyond which our predictions are only approximative; see text for more details). **d)**: Synthetic maps including the effect of an extinction screen towards L1551-IRS5. **e)**: Line profile extracted from the predicted PV diagram (Panel **c)**) at the position of PHK 1.

The synthetic images show that our cold disk wind model reproduces quite well the general observed morphology (although a higher extinction towards the source would be needed to hide completely the base of the jet). Interestingly, the sharp decrease in extinction at 1″ produces an emission peak close to the observed peak PHK 1. We also note that refocussing onto the jet axis in our model produces a peak at a distance comparable to the distance of knot PHK 2. In synthetic PV diagrams, the refocusing of streamlines produces a strong emission ridge beyond 2″ from the star, as the electronic temperature and density are locally enhanced by compression. The apparent deceleration in this ridge is due to the self-similarity of the solution: Streamlines of lower speeds are launched from larger disk radii, and thus recollimate farther from the star. A dashed curve in Fig. 7c shows the locus of the points where streamlines start to recollimate. Predictions downstream from this curve are only indicative, since gas pressure effects (neglected in the MHD solution) should eventually counteract compression, and start to have an important effect on the dynamics.

Figure 7e plots the synthetic line profile in the region before jet recollimation occurs. It shows that our cold disk wind model reproduces quite remarkably the main kinematical properties of the central regions of the L1551 jet: the observed velocity full width at zero intensity of 300 km s^{-1} (350 km s^{-1} in the model) as well as the existence of two velocity components: a high velocity component (HVC) and an intermediate-velocity component (IVC[2]) with centroid velocities −300 km s^{-1} (−360 km s^{-1} in the model), and −100 km s^{-1} (−160 km s^{-1} in the model) respectively. We stress in particular that a single cold disk wind model can fully account for the global kinematical properties, in particular the velocity extent of the profile, due to the range of streamlines involved. Streamlines originating from the disk inner truncation radius rapidly collimate, producing a fast narrow jet, while outer streamlines produce a wider angle slower wind accounting for the low-velocity part of the profile. As already pointed out in Cabrit et al. (1999) and Garcia et al. (2001b), a two component wind model, as earlier suggested by Kwan & Tademaru (1995), may not be necessary to account for both observed velocity peaks (HVC and IVC).

We notice however one important discrepancy between model and observations, apart from the apparent deceleration of the high-velocity emission ridge discussed earlier and due to the refocusing of streamlines towards the axis in the model. The relative intensity of the IVC and HVC at large distances is not well reproduced by the cold disk wind model. In the L1551 observations, the intermediate-velocity component dominates the emission out to 3″ from the star, while in the model the IVC emission drops rapidly beyond 0.5″. We note the possibility that the position-velocity diagram of Pyo et al. (2002) is contaminated by the southern L1551 jet (with line of sight velocities of ≃−60 km s^{-1}, Hartigan et al. 2000), especially at intermediate-velocity towards the PHK 1 knot where the two jets appear to merge in the images. However, following Pyo et al. (2002), we estimate this possibility unlikely at distances ≥1″ where the southern jet is several times fainter than the northern one.

---

[2] We use this denomination to differentiate the IVC from the true low velocity component observed in classical T Tauri stars which have much lower centroid velocities (−10 km s^{-1}) and are spatially unresolved.

We now apply the same type of comparison to DG Tau, an "extreme" T Tauri star with an infrared excess intermediate between Class I and Class II, and a particularly bright and well-studied optical jet (Lavalley-Fouquet et al. 2000; Dougados et al. 2000; Bacciotti et al. 2000). A direct comparison with models is possible since the jet inclination is known from proper motions, and high-resolution velocity-resolved [Fe II] 1.644 μm spectra were recently published by Pyo et al. (2003). In DG Tau, ejection signatures have been shown to be highly time variable close to the central source: Large changes in the measured velocity distribution, covering the range from 0 to -400 km s^{-1} , are observed at distances <0.5–1″ on timescales of a few years (Solf 1997). However, beyond these distances, terminal velocities varied by less than 20% over 10 years: -200 km s^{-1} at d = 3–3.5″ observed in Solf & Böhm (1993), -210 to -190 km s^{-1} at d = 2.5–4″ in Lavalley-Fouquet et al. (2000), -240 km s^{-1} at $d > 1.2''$ in Pyo et al. (2003). Internal shocks due to variability of the ejection velocity are expected to dissipate quickly along the jet (Raga & Kofman 1992), leaving the average flow mostly unperturbed at large distances. Indeed, derived shock velocities in the knots of the DG Tau jet do not exceed 50–70 km s^{-1} (Lavalley-Fouquet et al. 2000). A direct comparison of the properties of the jet on scales ≥100 AU with the predictions of stationary models appears therefore justified.

In Fig. 8, we compare the long-slit spectrum from Pyo et al. (2003) with our model predictions, convolved by the appropriate resolution (0.16″ and 30 km s^{-1}). We took an accretion rate of 10^{-6} $M_\odot$ yr^{-1}, close to the estimated value of 2×10^{-6} $M_\odot$ yr^{-1} through the disk (Hartigan et al. 1995) and an inclination angle of 45°, as estimated from the proper motions (Dougados et al. 2000; Pyo et al. 2003). The model again explains well the presence of two velocity components, and the general centroid velocities: the IVC peaks at ~ -60 to -130 km s^{-1} in DG Tau (-100 to -140 km s^{-1} in the model), the HVC peaks at -200 to -240 km s^{-1} in DG Tau (-360 km s^{-1} in the model). However, we note that the agreement for the HVC centroid is less good than in L1551-IRS5, in the sense that the model now overestimates the HVC velocity by a factor 1.5. Another discrepancy, also encountered in the case of L1551-IRS5, is that the IVC rapidly becomes weaker than the HVC in our model (at $Z \simeq 0.2''$), while in the observations of Pyo et al. (2003), the IVC dominates over the HVC much further out from the star (until $Z \simeq 0.6''$).

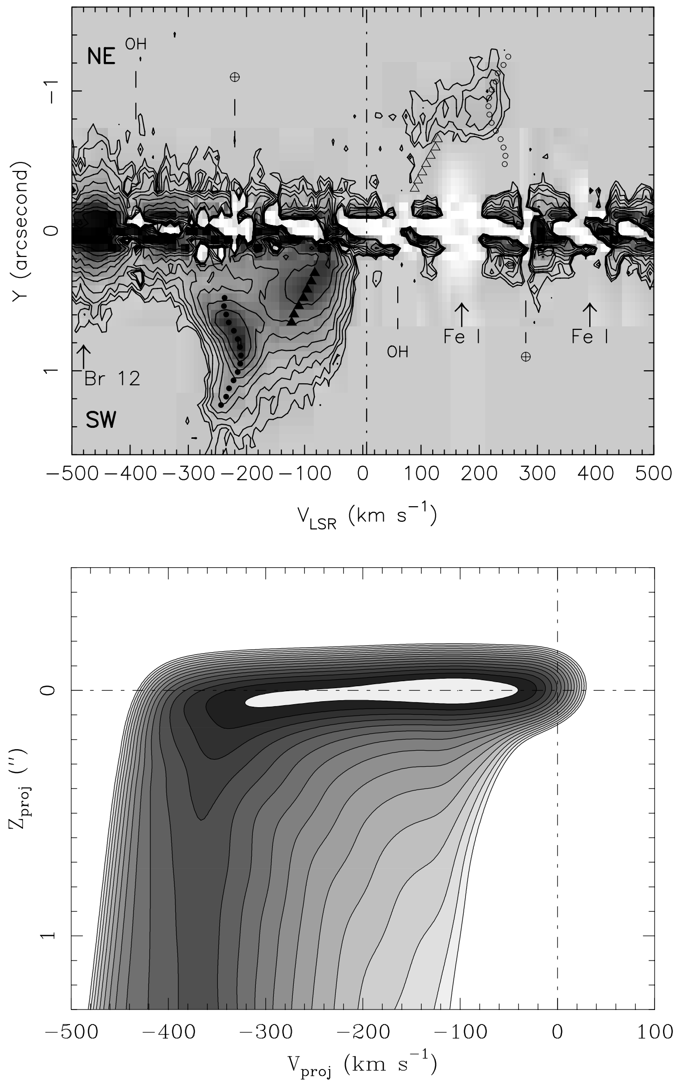

Fig. 8. [Fe II] 1.644 μm position-velocity diagrams. Contours are drawn with equal intervals in logarithmic scale. **Top**: Observations of the DG Tau jet (Pyo et al. 2003) with an angular resolution of 0.16″ and a velocity resolution of 30 km s^{-1}. **Bottom**: Predicted diagram from the cold disk wind model A (Garcia et al. 2001b) with ξ = 0.01, $\dot{M}_{\rm acc} = 10^{-6}$ $M_\odot$ yr^{-1}, i = 45°, convolved with the beam sizes of DG Tau observations.

3.3.2. Density

Itoh et al. (2000) derive the variation of extinction and $n_{\rm e}$ along the L1551 jet from JH-band spectroscopic observations, using the [Fe II] 1.257 μm/1.644 μm and 1.644 μm/1.533 μm line ratios (see Sect. 2.2). The derived electron densities decrease from 10^6 cm^{-3} (at d = 2″ = 280 AU from IRS5) to 10^4 cm^{-3} (d = 4″ from IRS5). For our fiducial cold disk wind model (with $\dot{M}_{\rm acc} = 10^{-5}$ $M_\odot$ yr^{-1}), we compute $n_{\rm e}$ from [Fe II] 1.644 μm/1.533 μm line ratios integrated across the jet. On the same spatial scales the predicted value is $\simeq 10^3$ cm^{-3}, i.e. 10 to 1000 times smaller than observed. We note that even assuming fully ionized gas (i.e. extra heating mechanisms: shocks or turbulent dissipation), the density in our model would still remain too low: all streamlines have $n_{\rm H} < 10^6$ cm^{-3} beyond Z = 100 AU for $\dot{M}_{\rm acc} = 10^{-5}$ $M_\odot$ yr^{-1} (see Fig. 5 with $\dot{M}_{\rm acc} = 10^{-6}$ $M_\odot$ yr^{-1}, and note that $n_{\rm H} \propto \dot{M}_{\rm acc}$). This density deficiency has already been observed in the central regions of T Tauri microjets (Lavalley-Fouquet et al. 2000; Garcia et al. 2001b). The near-IR observations of the L1551 jet show that self-similar *cold* disk winds also fail to reproduce the observed electronic densities in younger embedded flows on spatial scales of a few 100 AUs.

3.3.3. Summary

While the near-IR [Fe II] profiles predicted by the cold disk wind model reproduce rather well the two velocity components (HVC and IVC) observed in stellar jets, they appear to suffer from the same deficiency of intermediate-velocity emission (as compared to high-velocity) already noted in optical studies of the inner jet regions in T Tauri stars (Cabrit et al. 1999; Garcia et al. 2001b). More efficient heating at the base of the jet appears needed to enhance the brightness of the IVC component compared to the HVC. In addition, the predicted terminal velocity for the HVC appears in very good agreement (within ≃20%) with the observations in the Class I source L1551–IRS5, but exceeds the observed speed of the HVC by a factor ≃1.5 in the Class I/II source DG Tau. We note that the asymptotic poloidal velocity predicted by the disk wind models can be expressed by: $v_{\mathrm{pol},\infty} \simeq v_{\mathrm{K},0}\sqrt{2\lambda - 3}$, where $v_{\mathrm{K},0}$ is the Keplerian speed in the disk midplane at the cylindrical launching radius r_0 and $\lambda \simeq r_{\mathrm{A}}^2/r_0^2$ the magnetic lever arm (r_{A} is the radius of the magnetic surface at the Alfvén point). Lower terminal poloidal velocities can be achieved by decreasing either $v_{\mathrm{K},0}$ (i.e. increasing r_0) or λ. Larger launching radii would lead however to even lower total jet densities, increasing the discrepancy with the observations. Therefore, smaller magnetic lever arms (typically $\lambda < 25$ as compared to our disk wind solution where $\lambda \simeq 50$) are required to reproduce the observed terminal speed in DG Tau.

4. Conclusions

Thanks to a simplified 16-level atomic model, we investigated the potential of near-IR [Fe II] lines as diagnostics of physical conditions in the inner regions of stellar jets. We presented diagnostic diagrams that provide determinations of n_{e} in the range 10^2 to 10^5 cm^{-3}, T_{e} below 20 000 K, and a lower limit to the Fe/S ratio (based on a near-infrared [Fe II]/[S II] line ratio). Using observational data from Nisini et al. (2002) in several HH flows, and assuming $T_{\mathrm{e}} \simeq 7000$ K, we deduce lower limits to the iron gas phase abundance comparable to those found from molecular shock models by Nisini et al. (2002), i.e. on average 30% of the solar value. For $T_{\mathrm{e}} \simeq 10^4$ K, the derived Fe abundances would be roughly solar in most HH objects, except HH 111H and HH 241A. Hence, we confirm earlier work indicating an efficient dust destruction mechanism in stellar jets. However, we cannot yet conclude on the nature of the grain destruction process, i.e. shocks versus evaporation. Calculations of grain destruction in hydrodynamic shocks have concentrated so far on the low-density interstellar medium (Jones et al. 1994) and similar computations with preshock densities ≃10^3–10^4 cm^{-3} typical of HH flows are needed. Such calculations currently exist only in the case of low-ionization magneto-hydrodynamics shocks with ion-neutral decoupling, but this type of shocks may not occur at the ionization level of a few % observed in optical jets. High angular resolution observations of the jet base in [Fe II] and [S II] lines, e.g. with NAOS/CONICA on the VLT, are also needed to determine whether the grains are destroyed in the vinicity of the exciting source or further out.

In the second part of this article, we extended the work presented in Garcia et al. (2001b) to predictions in the near-infrared domain, by applying our Fe$^+$ emissivity calculations to a cold disk wind model with a self-consistent thermal and ionization structure (Ferreira 1997; Garcia et al. 2001a). On large scale (a few 100 AUs), predicted emission maps are very similar in near-IR [Fe II] lines and optical [S II] lines. However, on scales of 1 AU soon accessible with the AMBER/VLTI instrument, [Fe II] lines appear more efficient to trace colder and more extincted regions very close to the driving source. In particular, AMBER/VLTI observations in [Fe II] lines are predicted to resolve the innermost streamline and inner hole expected for a cold disk wind.

Comparing synthetic maps with recent observations of the L1551–IRS5 and DG Tau jets in near-infrared [Fe II] lines, we find that our model is in good agreement with the global kinematics, and notably the presence of two velocity components: an intermediate-velocity component (IVC) at −100 km s^{-1} (−100 to −150 km s^{-1} in the model) and a high-velocity component (HVC) at −230 to −300 km s^{-1} (−360 km s^{-1} in the model). However, the predicted velocity for the HVC tends to be too high (by 20% only in L1551 IRS5, but by a factor 1.5 in DG Tau). Furthermore, the model predicts insufficient emission at intermediate-velocity, compared to the HVC, and also insufficient gas density in L1551. Similar failures were encountered when comparing the cold disk wind model with observations of jets from T Tauri stars in the optical domain (Garcia et al. 2001b). MHD disk wind models with entropy injection at the base of the jet (Casse & Ferreira 2000) appear promising to solve these problems as they could provide denser solutions, with a slower HVC and more emission from the IVC (originating from the warm wind base). Calculations of observational predictions for this class of “warm disk winds” are in progress and will be the subject of a future paper.

Acknowledgements. We are very grateful to Anil Pradhan for communicating unpublished results from his 142-level code and for useful suggestions. We would like to thank the referee, K.-H. Böhm, for his helpful comments.

References

Bacciotti, F., & Eislöffel, J. 1999, A&A, 342, 717
Bacciotti, F., Mundt, R., Ray, T. P., et al. 2000, ApJ, 537, L49
Beck-Winchatz, B., Böhm, K. H., & Noriega-Crespo, A. 1994, PASP, 106, 1271
Beck-Winchatz, B., Böhm, K. H., & Noriega-Crespo, A. 1996, AJ, 111, 346
Blandford, R. D., & Payne, D. G. 1982, MNRAS, 199, 883
Böhm, K.-H., & Solf, J. 1990, ApJ, 348, 297
Burrows, C. J., Stapelfeldt, K. R., Watson, A. M., et al. 1996, ApJ, 473, 437
Cabrit, S., Edwards, S., Strom, S. E., & Strom, K. M. 1990, ApJ, 354, 687
Cabrit, S., Ferreira, J., & Raga, A. C. 1999, A&A, 343, L61
Cabrit, S. 2002 in Star Formation and the Physics of Young Stars, ed. J. Bouvier, & J. P. Zahn, EAS Publ. Series, 3, 147
Cai, W., & Pradhan, A. K. 1993, ApJS, 88, 329
Casse, F., & Ferreira, J. 2000, A&A, 361, 1178

Cohen, M., Bieging, J. H., & Schwartz, P. R. 1982, ApJ, 253, 707

Dougados, C., Cabrit, S., Lavalley, C., & Ménard, F. 2000, A&A, 357, L61

Ferreira, J., & Pelletier, G. 1995, A&A, 295, 807

Ferreira, J. 1997, A&A, 319, 340

Fridlund, C. V. M., & Liseau, R. 1998, ApJ, 499, L75

Fritzsche, S., Fricke, B., Geschke, D., Heitmann, A., & Sienkiewicz, J. E. 1999, ApJ, 518, 994

Garcia, P. J. V., Ferreira, J., Cabrit, S., & Binette, L. 2001, A&A, 377, 589, Paper I

Garcia, P. J. V., Cabrit, S., Ferreira, J., & Binette, L. 2001, A&A, 377, 609, Paper II

Hartigan, P., Morse, J., & Raymond, J. 1994, ApJ, 436, 125

Hartigan, P., Edwards, S., & Ghandour, L. 1995, ApJ, 452, 736

Hartigan, P., Morse, J., Palunas, P., Bally, J., & Devine, D. 2000, AJ, 119, 1872

Hirth, G. A., Mundt, R., & Solf, J. 1997, A&AS, 126, 437

Hollenbach, D., & McKee, C. F. 1989, ApJ, 342, 306

Itoh, Y., Kaifu, N., Hayashi, M., et al. 2000, PASJ, 52, 81

Jones, A. P., Tielens, A. G. G. M., Hollenbach, D. J., & McKee, C. F. 1994, ApJ, 433, 797

Kwan, J., & Tademaru, E. 1995, ApJ, 454, 382

Lavalley-Fouquet, C., Cabrit, S., & Dougados, C. 2000, A&A, 356, L41

Momose, M., Ohashi, N., Kawabe, R., Nakano, T., & Hayashi, M. 1998, ApJ, 504, 314

Nisini, B., Caratti o Garatti, A., Giannini, T., & Lorenzetti, D. 2002, A&A, 393, 1035

Nussbaumer, H., & Storey, P. J. 1988, A&A, 193, 327

Osterbrock, D. E. 1989, Astrophysics of Gaseous Nebulae and Active Galactic Nuclei (Mill Valley: Univ. Science Books)

Pradhan, A. K., & Zhang, H. L. 1993, ApJ, 409, L77

Pyo, T., Hayashi, M., Kobayashi, N., et al. 2002, ApJ, 570, 724, Erratum, `http://www.subarutelescope.org/staff/pyo/L1551paper/Erratum.pdf`

Pyo, T.-S., Kobayashi, N., Hayashi, M., et al. 2003, ApJ, 590, 340

Raga, A. C., & Kofman, L. 1992, ApJ, 386, 222

Reipurth, B., Yu, K. C., Heathcote, S., Bally, J., & Rodríguez, L. F. 2000, AJ, 120, 1449

Rodríguez, L. F., Curiel, S., Cantó, J., et al. 2003, ApJ, 583, 330

Savage, B. D., & Sembach, K. R. 1996, ARA&A, 34, 279

Shang, H., Shu, F. H., & Glassgold, A. E. 1998, ApJ, 493, L91

Shang, H., Glassgold, A. E., Shu, F. H., & Lizano, S. 2002, ApJ, 564, 853

Sofia, U. J., & Meyer, D. M. 2001, ApJ, 554, L221

Solf, J., & Böhm, K. H. 1993, ApJ, 410, L31

Solf, J. 1997, in Herbig-Haro Flows and the Birth of Stars, ed. B. Reipurth, & C. Bertout (Kluwer Academic Publishers), IAU Symp., 182, 63

Verner, E. M., Verner, D. A., Baldwin, J. A., Ferland, G. J., & Martin, P. G. 2000, ApJ, 543, 831

Zhang, H. L., & Pradhan, A. K. 1995, A&A, 293, 953